Accelerated propagation of Stokes pulses in a Brillouin fiber laser: pump power dependence of cavity modes

R. K. Pattnaik* and Jean Toulouse

Physics Department, Lehigh University Bethlehem, Bethlehem, Pennsylvania 18015, USA
*Corresponding author: rkp2@lehigh.edu

We investigate both experimentally and numerically the evolution of slow light in the limit of high stimulated-Brillouin-scattering gain, as in a Brillouin fiber laser. The Stokes pulse transit time is measured to decrease and the resonant modes to shift to higher frequencies with increasing pump power. Numerical simulations reveal that pump depletion introduces a nonuniform group index across the Stokes pulse as it interacts with the pump, the index being greater for the leading edge and decreasing progressively towards the trailing edge in proportion to the remaining pump power. This results in a progressive acceleration of the Stokes pulse from slow to fast as it propagates through the cavity. © 2008 Optical Society of America

OCIS codes: 290.5830, 190.5890, 140.3510.

1. INTRODUCTION

Stimulated Brillouin scattering (SBS) is one of the most prominent nonlinear effects in optical fibers because of its low excitation threshold with a narrowband pump. The Brillouin scattered light arises from the scattering of a pump wave off the copropagating acoustic wave in the medium. Using continuous wave (CW) excitation, a few milliwatts of pump power is sufficient to excite SBS, leading to a counterpropagating Stokes wave. Due to its fundamental interest [1–5] as well as its practical implications [6], this three wave interaction—optical pump, Stokes, and acoustic waves—has been investigated in great depth. Although SBS can be a negative or detrimental effect for the transmission of optical signals through fibers [7–9], it nevertheless is of special interest for fundamental studies of light–matter interaction and also forms the basis for very useful applications such as narrowband lasers [10,11], optical modulation, and, as discovered relatively recently, slow light [12–15] in optical delay lines, which has been reviewed by Boyd and Gauthier [16].

The latter application has been made possible by the recent discovery of the SBS-induced slowing down of optical signals in fibers. As with other resonant interactions SBS exhibits dispersion within the bandwidth of the resonance [16]. In the low-gain limit the group index (in the spectral region of the SBS resonance) increases with pump power (or equivalently with gain), causing a slowing down of the Stokes wave (slow light). As demonstrated in [12–14] the group velocity of a signal pulse propagating in a fiber SBS amplifier can be delayed by several nanoseconds, depending on gain, fiber type, and length. However, in the studies cited above, slow light has been achieved in the low-gain limit in an amplifier configuration. Various authors have noted that, as the gain increases, the slow-light effect saturates and pulse advance-

ment rather than pulse slowing down occurs. However, none have investigated in detail the evolution of this effect in the high-gain regime of a Brillouin laser, and in particular the effect of pump depletion on dispersion.

In the present paper we report a numerical and experimental study of the effect of pump depletion on the propagation characteristics of Stokes pulses and on their spectrum in a Brillouin fiber laser. In this laser the Stokes pulses are generated from the spontaneously (Brillouin) scattered light and evolve into a coherent emission when the pump power exceeds the SBS threshold [4]. Simulation and experimental results show that, in the limit of high-gain above the SBS threshold, Stokes pulses are (re)accelerated and that, as a consequence, the resonant cavity modes shift towards higher frequencies. In the following, we first briefly review the theory of slow light as it is applicable in a low-gain medium such as a Brillouin amplifier [12–14]. We then present experimental results in the high-gain limit of a Brillouin laser. Finally, we outline our numerical model, present the simulation results, and compare them with the experimental ones.

2. NORMAL DISPERSION ASSOCIATED WITH A BRILLOUIN RESONANCE AND SLOW LIGHT

When the external feedback from Fresnel reflections at the fiber ends is included in the SBS dynamics the fiber forms a laser cavity and, if the pump intensity is above a certain threshold, the Brillouin scattered light evolves into coherent laserlike radiation [10,17,18]. The spectrum of this Brillouin laser exhibits modes at regular frequency intervals equal to the cavity free spectral range (FSR) [10,11]. The SBS process can be described by one-dimensional coupled wave equations. Using the slowly varying amplitude approximation in the small gain (un-

depleted pump) limit, the effective refractive index, including the nonlinear contribution, is given by [14]

$$n_{\text{eff}} = n(\omega) + g \frac{c}{\omega} \frac{\Delta\Omega}{\Gamma_B} I_L, \tag{1}$$

where $n(\omega)$ is the normal refractive index; $\Delta\Omega = \omega - (\omega_L - \Omega_B)$ is the detuning with $\Omega_B = qV_B$, V_B being the acoustic speed; I_L is the pump intensity (assumed undepleted); Γ_B is the damping of the acoustic wave; and the Brillouin coefficient is given by [6]

$$g = g_B \frac{(\Gamma_B/2)^2}{(\Gamma_B/2)^2 + (\Delta\Omega)^2}, \tag{2}$$

where g_B is the line-center Brillouin gain. The group index, defined by $n_g = n_{\text{eff}} + \omega d n_{\text{eff}}/d\omega$ is given by [14]

$$n_g = n_{g0}(\omega) + \frac{g_B c I_L \Gamma_B}{4} \frac{(\Gamma_B/2)^2 - (\Delta\Omega)^2}{((\Gamma_B/2)^2 + (\Delta\Omega)^2)^2} \approx n_{g0}(\omega) + \frac{g_B c I_L}{\Gamma_B}, \tag{3}$$

where $n_{g0}(\omega) = n(\omega) + \omega d n/d\omega$, is the group index in the absence of SBS coupling. From Eqs. (1) and (3) it is evident that the effective refractive index exhibits normal dispersion. For $\Delta\Omega < \Gamma_B$ the group index increases with the pump intensity, I_L, and the group velocity, $v_g = c/n_g$, decreases accordingly, leading to slow light. The change in group index due to SBS has been estimated [13,14] to be of the order of 10^{-3}. However, this estimate is only valid in the small gain limit, i.e., when pump depletion is neglected. In the high-gain limit, pump depletion can no longer be neglected and the dispersion is modified in a new and interesting way, leading to a reacceleration of the Stokes wave.

This modified dispersion at high Brillouin gain is readily observed in the spectrum of a Brillouin laser. The group velocity (or group index), which determines the FSR [19,20] of the laser cavity, is given by

$$\Delta\nu = \frac{c}{2n_g L} = \frac{v_g}{2L}, \tag{4}$$

where n_g is the group index, L is the length of the Fabry–Pérot fiber cavity, and v_g is the group velocity. From Eq. (4), it is clear that the FSR will increase or decrease in response to changes in group velocity with pump power or gain. In this paper we first investigate experimentally the pump power dependence of the lasing modes in a Brillouin fiber laser and then provide a model to explain the observation. Thus, the object of this study is to examine the propagation of a Stokes wave in a Brillouin laser configuration, i.e., in the presence of pump depletion, and to discuss the ensuing effects on the spectrum of the (Brillouin) laser. We first present the experimental results, then describe the numerical simulation model, and finally discuss the experimental results in light of the simulation results.

3. EXPERIMENT AND RESULTS

The experimental setup is shown in Fig. 1. The output of an external cavity laser (ECL) at 1550 nm was amplified
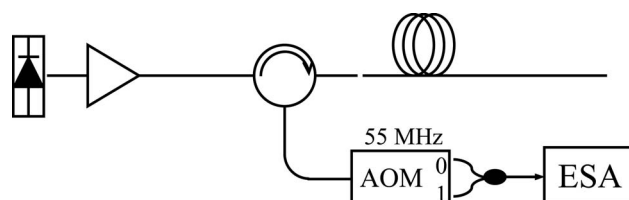

Fig. 1. Schematic of the experimental setup. The test fiber was 500 m long and was butt-coupled to the output of the circulator. The AOM was used to shift the frequencies of the modes by 55 MHz.

and butt-coupled into a 500 m long fiber that had an attenuation of about 0.5 dB/km. Care was taken to leave a small but nonzero gap between the test fiber and the circulator in order to form a cavity. Both ends of the test fiber were flat cleaved to form the laser resonator. As is shown later, when the pump power exceeded the threshold the SBS emission evolved into a coherent train of Stokes pulses. This emission, propagating (backward) through the circulator, was first recorded on a digitizing oscilloscope to measure the transit time of the pulses through the fiber resonant cavity. Due to the narrowness of the FSR (about 200 kHz) of the fiber resonator, a heterodyne technique was used to record the spectrum with sufficient resolution. The modes were first shifted down to a lower frequency by injecting the backscattered Stokes emission into a 55 MHz acousto-optic modulator (AOM). The first-order output from the AOM was then mixed with its unshifted (zeroth-order) output and the resulting beat signal was recorded on a rf electrical spectrum analyzer (ESA). This technique enabled displaying the beat spectrum with the central lasing mode at 55 MHz. The threshold pump power for lasing, determined by monitoring the spectrum of the reflected light, was found to be 23 dBm. The measurements reported here are mostly for pump powers above this threshold.

In Fig. 2 we present the time-domain traces of the laser emission recorded on a digitizing oscilloscope. The output is seen to consist of periodic pulses, characteristic of the transmission through a Fabry–Pérot cavity (here the SBS fiber laser cavity). The significant point to note in these time-domain traces is the decreasing Stokes pulse period with pump power. In Fig. 2(a) the period is 4.74 μs for an input pump power of 23.2 dBm ($\sim$209 mW), but it decreases to 4.6 μs [Fig. 2(b)] as the pump power is raised to 24 dBm ($\sim$251 mW). According to Eq. (4) this corresponds to a 3% decrease in the group velocity of the Stokes pulse for an increase of 0.8 dB or 17% in pump power. Also visible in both traces, the leading edge rises slightly more sharply or faster than the trailing edge.

The dependence of the Stokes pulse period on pump power implies that the frequency of the lasing (or cavity) modes or the associated FSR also depends on pump power. This can be seen experimentally by displaying the cavity modes on the ESA and is shown in Fig. 3(a) for two pump powers. The spectrum consists of many orders, but the figure includes modes only up to the third harmonic for clarity. Due to the choice of heterodyning frequency the fundamental mode (with mode index m_0) appears at 55 MHz and the other higher-order modes are symmetrically spaced on either side, according to the FSR of the 500 m long fiber cavity.
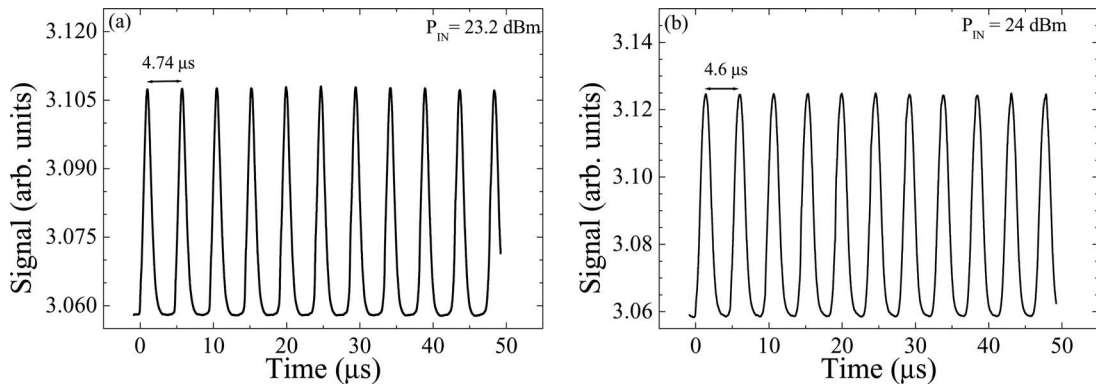
Fig. 2. Oscilloscope traces of Stokes pulses at the output end as a function of time. (a) is the result of 23.2 dBm and (b) of 24 dBm of input power. The period in (a) is 4.74 μs while in (b) it is 4.6 μs. The period decreases by about 0.1 μs as the input power is increased.

Figure 3(a) clearly shows the mode separation or the FSR increasing with pump power. It is about 212.5 kHz for an input power of 23.8 dBm (solid curve) and increases to 217 kHz for 24.8 dBm (dotted curve), which corresponds to a shift of nearly 2.4% for a 1 dB increase in pump power. The shift of each mode (relative to the fundamental mode) is also found to increase with its order. As seen more clearly in Fig. 3(b), the shift of the third harmonic is about 5.7 kHz whereas the second harmonic shifts by about about 3.2 kHz. The inset in Fig. 3(b) summarizes the frequency shifts of the first three harmonics with increasing pump power. (In this inset each harmonic has been normalized to its corresponding value at 200 mW.) This increase of the FSR indicates that the pulse propagation or group velocity is accelerated with increasing pump power in the lasing regime of SBS. A similar observation has been reported by Dämmig and Mitschke [20] with fibers with different reflectivities.

In Fig. 4, we display similar measurements, this time made on two photonic crystal fibers (PCF). The first one was made on 500 m of an RB61 fiber [Optical Fiber Solutions (OFS), Murray Hill, New Jersey, US] with parameters: $d_c=8$ μm, $d_H=1.85$ μm, and pitch $\Lambda=4.9$ μm. The second one was made on 500 m of an RB65 (OFS) fiber with parameters: $d_c=3.55$ μm, $d_H=1.15$ μm, and pitch Λ $=2.35$ μm. The RB61 fiber had a large core, nearly the same as that of a single-mode fiber (SMF), whereas RB65 had a much smaller core. The RB65 fiber also had a much

larger attenuation (about 20 dB/km at 1550 nm) than the RB61 fiber (about 2 dB/km). Nonetheless, even with high attenuation, SBS and the cavity modes were observed for pump powers exceeding the SBS threshold. Because of their high intrinsic losses the measurements on these two fibers were made without an AOM but taking advantage of the fact that the Stokes signal heterodyned with a small backreflected fraction of the incident light, still allowing detection using the ESA.

In Fig. 4 the intensity of the modes is seen to decrease with increasing order, and their frequency separation to increase with increasing pump power. The shifts of the second harmonics are displayed more clearly in the insets. For nearly the same increase in pump power ($\sim$1 dB), the shift is found to be significantly greater for the smaller core RB65 fiber than for the larger core RB61 fiber (12 versus 5.6 kHz). This difference can be attributed to the combination of a smaller effective group index and a shorter effective length due to the higher attenuation in RB65. Recent simulations of these two fibers have indeed shown that the optical mode becomes more sensitive to the fiber structure, and in particular to the holey cladding, as the core diameter or equivalently d/Λ decreases [21].

The results presented above for three different fibers clearly illustrate the dependence of the frequency of the cavity modes or FSR on pump power in a Brillouin fiber laser. From Eq. (4) we see that the only parameter that is
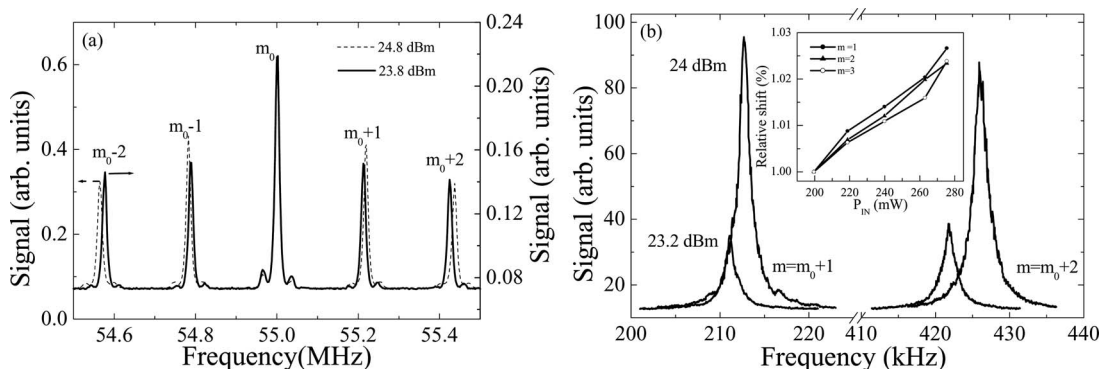

Fig. 3.   (a) Spectrum of the lasing modes (to the third harmonic) in a 500 m long fiber Brillouin laser. The fundamental or the first harmonic (labeled by the integer m_0) is at 55 MHz. Note that the harmonics shift to higher frequencies as the pump power is increased. (b) Expanded view of the second and third harmonics for two pump powers. As the pump power is increased, the frequency shift increases with the order of the harmonic mode. Inset: increase of frequency (in percent) of the three harmonics with pump power.
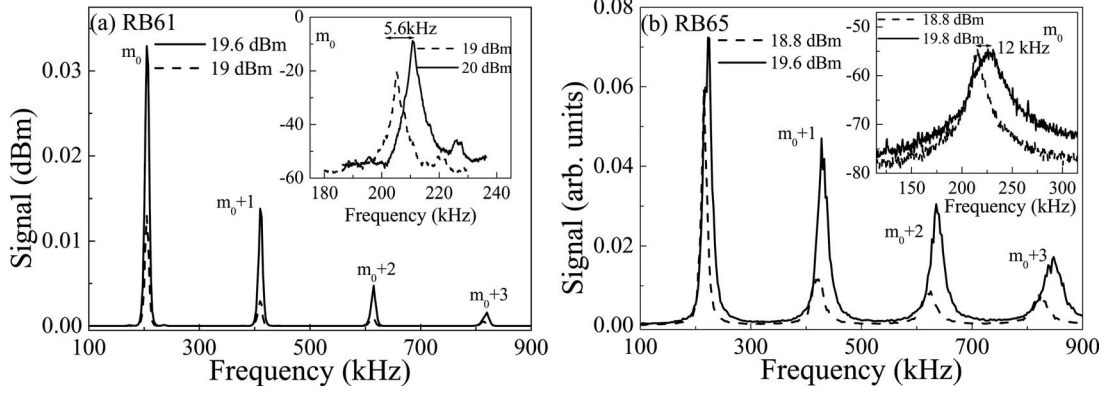
Fig. 4.   Pump power dependence of the resonant modes in PCF. As the pump power is increased, the gain increases and modes shift to higher frequencies. Expanded view is provided in the inset.

susceptible to change with pump power is the group velocity (there is no conceivable reason for the length of the fiber to decrease). We can therefore conclude that, in the high-gain regime of a Brillouin laser, this upward shift in frequency of the cavity modes, or of the FSR, is due to an increase in group velocity with pump power, in contrast to the results obtained in the undepleted pump regime in which the group velocity was found to decrease with increasing pump power. Two previous authors, Dämmig *et al.* [22] and Picholle *et al.* [23], did notice the increase in group velocity with gain but did not elaborate on it. In a later communication Dämmig and Mitschke [20] reported observations similar to ours. They used an analytic approach (in Brillouin amplifier configuration) to show that the propagation velocity increases with pump power. Here we use a numerical approach to study the three wave interaction in a resonator configuration. Moreover, our approach provides insight into the evolution of the Stokes pulse with time and space along with the variation of the group index in the pump depletion regime.

4. THEORY

We consider a fiber of length L in which a pump beam counterpropagates relative to the Stokes beam. The dynamics can be described by one-dimensional coupled wave equations [14,17,24,25] involving a backward pump wave $(1/2)\{E_L(z,t)\exp(-i(\omega_L t + k_L z)) + \text{c.c.}\}$, a forward Stokes wave $(1/2)\{E_S(z,t)\exp(-i(\omega t - kz)) + \text{c.c.}\}$ and a backward acoustic wave $(1/2)\{\rho(z,t)\exp(-i(\Omega t + qz)) + \text{c.c.}\}$. Using the slowly varying amplitude approximation, the three coupled wave equations can be written as [4,6,14]

$$-\frac{\partial E_L}{\partial z} + \frac{n_{g0}}{c}\frac{\partial E_L}{\partial t} + \frac{\alpha}{2}E_L = i\frac{\omega_L \gamma_e}{4cn\rho_0}\rho E_S, \qquad (5)$$

$$\frac{\partial E_S}{\partial z} + \frac{n_{g0}}{c}\frac{\partial E_S}{\partial t} + \frac{\alpha}{2}E_S = i\frac{\omega_L \gamma_e}{4cn\rho_0}\rho^* E_L, \qquad (6)$$

$$\frac{\partial \rho}{\partial t} + \left(\frac{\Gamma_B}{2} + i\Delta\Omega\right)\rho = i\frac{\epsilon_0 \Omega_B \gamma_e}{4V_a^2}E_L E_S^*, \qquad (7)$$

where, as before, $\Delta\Omega = \omega - (\omega_L - \Omega_B)$ is the detuning, n is the phase (modal) index [14], $\Gamma_B/2\pi$ is the FWHM of the spontaneous Brillouin gain spectrum, γ_e is the electros-

trictive coefficient, α is the attenuation, and ρ_0 is the undisturbed density. Zhu *et al.* [14] have studied in detail a numerical solution of Eqs. (5)–(7) in a Brillouin amplifier configuration while the present study involves a fiber resonator or a Brillouin laser. In the adiabatic approximation [17,18], according to which the amplitude of the pump and Stokes waves do not change significantly during a phonon lifetime, the inertial term, $\partial\rho/\partial t$ in Eq. (7) can be neglected. Furthermore, expressing the complex optical field amplitudes in the modulus-phase form $[E_L(z,t) = A_L e^{i\phi_L}, E_S(z,t) = Ae^{i\phi}]$ and making use of Eq. (2), we can rewrite the coupled wave equations in the following form:

$$-\frac{\partial A_L}{\partial z} + \frac{n_{g0}}{c}\frac{\partial A_L}{\partial t} + \frac{\alpha}{2}A_L = -\frac{\Gamma_B}{4}\frac{g_B\Gamma_B/2}{(\Gamma_B/2)^2 + \Delta\Omega^2} \approx -\frac{1}{2}g_B I A_L, \qquad (8)$$

$$\frac{\partial A}{\partial z} + \frac{n_{g0}}{c}\frac{\partial A}{\partial t} + \frac{\alpha}{2}A = \frac{\Gamma_B}{4}\frac{g_B\Gamma_B/2}{(\Gamma_B/2)^2 + \Delta\Omega^2} \approx \frac{1}{2}g_B I_L A, \quad (9)$$

$$-\frac{\partial\phi_L}{\partial z} + \frac{n_{g0}}{c}\frac{\partial\phi_L}{\partial t} = -\frac{\Gamma_B}{4}\frac{g_B\Delta\Omega}{(\Gamma_B/2)^2 + \Delta\Omega^2}I \approx \frac{g_B\Delta\Omega}{\Gamma_B}I, \qquad (10)$$

$$\frac{\partial\phi}{\partial z} + \frac{n_{g0}}{c}\frac{\partial\phi}{\partial t} = \frac{\Gamma_B}{4}\frac{g_B\Delta\Omega}{(\Gamma_B/2)^2 + \Delta\Omega^2}I_L \approx \frac{g_B\Delta\Omega}{\Gamma_B}I_L, \qquad (11)$$

where we have assumed that $\Delta\Omega^2(\ll \Gamma_B^2/4)$ can be neglected; g_B is the line-center Brillouin gain; and I and I_L are the intensities of the Stokes and pump beams, respectively. Several authors [23,26–31] have studied Eqs. (8) and (11) revealing many interesting features associated with the SBS dynamics. Our investigation here is to study how the pump depletion influences the velocity of the Stokes pulses in a narrow range of pump powers (about a decibel) above the SBS threshold. To this effect, we recall that the group delay, T_d, is given by $d\phi/d\omega$, which is also the difference in transit time in the presence and absence of SBS interaction. Thus we note that

$$T_d = \frac{\mathrm{d}\phi}{\mathrm{d}\omega} = \frac{L}{v_g} - \frac{L}{v_{g0}} = \frac{L}{c}\Delta n_g, \qquad (12)$$

where L is the length of the fiber; v_g and v_{g0} are, respectively, the group velocity in the presence and in the absence of the SBS interaction; and $\Delta n_g = n_g - n_{g0}$ is the change in group index due to SBS. The delay or change in group index as a function of pump power can then be directly obtained from Eq. (11) [using Eq. (12)] as

$$\frac{\partial T_d}{\partial z} + \frac{n_{g0}}{c}\frac{\partial T_d}{\partial t} = \frac{g_B \Gamma_B}{4}\frac{(\Gamma_B/2)^2 - \Delta\Omega^2}{[(\Gamma_B/2)^2 + \Delta\Omega^2]^2}I_L \approx \frac{g_B}{\Gamma_B}I_L, \quad (13)$$

which, in the steady state and undepleted pump approximation, readily gives

$$T_d = \frac{g_B L}{\Gamma_B}I_L = \frac{G}{\Gamma_B}, \qquad (14)$$

showing that that the delay is proportional to the SBS gain, $G = g_B I_L L$ [14]. However, as pointed out in Section 1, pump depletion cannot be ignored in a Brillouin laser operating in the high SBS gain limit. Therefore, in order to predict the behavior of the group velocity and its dependence on pump power, it is necessary to solve the coupled equations (8), (9), and (13) without making the common approximation of an undepleted pump. To do this, we begin by rewriting the equations in a dimensionless form in terms of normalized amplitudes,

$$-\frac{\partial a_L}{\partial\xi} + \frac{\partial a_L}{\partial\tau} + \frac{\alpha L}{2}a_L = -\frac{1}{2}Ga^2 a_L, \qquad (15)$$

$$\frac{\partial a}{\partial\xi} + \frac{\partial a}{\partial\tau} + \frac{\alpha L}{2}a = \frac{1}{2}Ga_L^2 a, \qquad (16)$$

$$\frac{\partial\Delta n_g}{\partial\xi} + \frac{\partial\Delta n_g}{\partial\tau} = \frac{Gc}{L\Gamma_B}a_L^2, \qquad (17)$$

where $a_L = A_L/A_{L0}$ and $a = A/A_{L0}$ represent, respectively, the normalized pump and Stokes amplitudes, A_{L0} being the amplitude of the pump injected at $z = L$. The length and time in Eqs. (8), (9), and (13) have also been normalized according to $\xi = z/L$ and $\tau = t/T$, with L being the length of the fiber and $T = nL/c$ being the one-way-trip transit time (n is the normal unmodified group index and c is the speed of light). In writing Eq. (17) we have used the right-hand side of Eq. (12) to express T_d in terms of Δn_g. We have solved these equations numerically, following the method of characteristics and using a standard fourth-order Runge–Kutta algorithm with the following boundary conditions [18] (see Fig. 5):

$$a(0,\tau) = f(0,\tau) + (R_1 R_2 e^{-\alpha L/2})a(L,\tau-1),$$

$$a_L(L,\tau) = 1 + (R_1 R_2 e^{-\alpha L/2})a_L(0,\tau-1), \qquad (18)$$

where R_1 and R_2 represent the amplitude reflectivity coefficients at the end faces of the fiber. We assumed R_1 and R_2 to be equal and renamed their product as the reflection coefficient squared, R^2. $f(0,\tau)$ is a (normalized) seed signal initiating the SBS process, which may be interpreted [4]
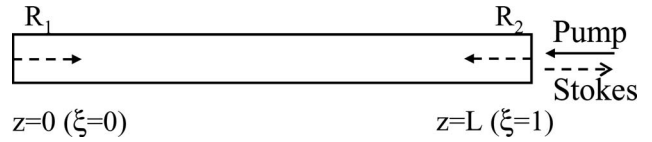

Fig. 5. Schematics of the Fabry–Pérot Brillouin fiber laser. The pump is injected from the right. R_1 and R_2 are the amplitude reflectivities of the end faces. The initial CW Stokes emission (dotted arrows) evolving from the noise near the left end face develops into resonant modes upon Fresnel reflection from the end faces.

as the amplitude of the spontaneous Brillouin signal due to the pump beam close to $z = 0$. The strength of this seed signal has been taken to be of the order of a nanowatt or lower in the numerical results reported by others [4,32]. In our simulations, the fiber under test was assumed to be a standard SMF-28 fiber and the relevant parameters used in the simulation are given in Table 1.

Before discussing the simulation results, following Tang [2] we may point out that the strong damping approximation [neglecting $\partial\rho/\partial t$ in Eq. (7)] is valid as long as the pulse duration of the pump or Stokes wave is greater than the phonon lifetime (of the order [1–3] of 10 ns at room temperature). In our simulations the pump is a CW and (as will be shown later) the Stokes pulse duration is of the order of a few microseconds. We can therefore safely neglect the inertial term, $\partial\rho/\partial t$, in Eq. (7).

The simulation results presented in Section 5 show that, in a Brillouin laser configuration, the group velocity of a Stokes pulse is enhanced—or, equivalently, reaccelerated—as the gain is increased. In the frequency domain this results in an increase of the FSR of the fiber laser.

5. NUMERICAL RESULTS

To understand the numerical results presented here it is important to stress that our simulations assumed a CW pump injected at $z = L$ (far end of the fiber) and counter-propagating relative to Stokes pulses originating from $z = 0$ (near end of the fiber). In a first simulation, we calculated the transmitted and reflected powers as a function of input pump power by solving the set of equations (15)–(17). This was important for two reasons; first, it helped establish the consistency of our simulations and, second, it allowed us to determine the SBS threshold, thus providing a metric of what represented low and high-gain. Moreover, it also provided a reference for the subsequent simulations in the depleted pump regime. In Fig. 6(a) we present the results of these first simulations, transmitted and reflected powers being defined here as the average power of the Stokes emission at $z = L$ and the average pump power at $z = 0$ as a function of input power. As the input power exceeds the SBS threshold of 30 mW, the Stokes power is seen to rapidly increase and the out-

Table 1. Fiber Parameters for Simulation

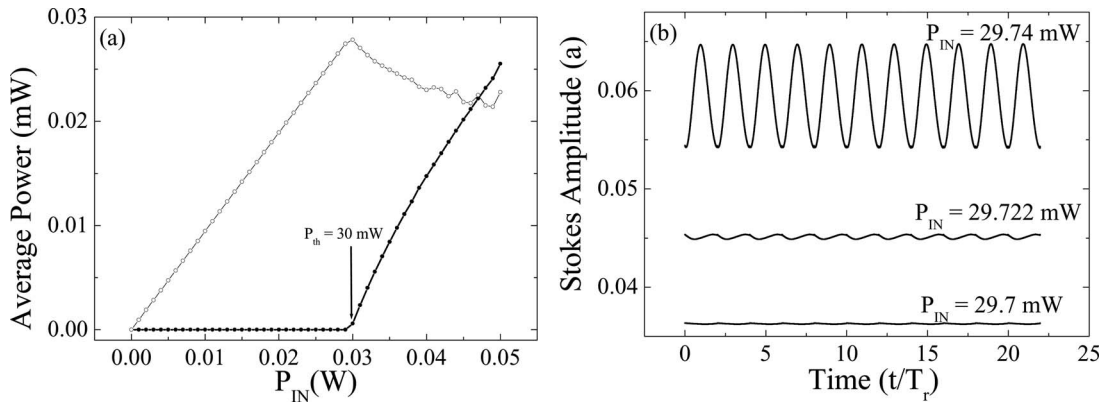| L (m)	α (m^{-1})	g_B (m/W)	A_{eff} (μm^2)	R	$\Gamma_B/2\pi$ (Hz)	$f(0,\tau)$
500	0.115×10^{-3}	2.5×10^{-11}	55	0.04	20×10^6	1×10^{-6}

Fig. 6.   (a) Simulation results for the average reflected power (solid circles) and the transmitted power (open circles) for a 500 m long SMF fiber. The SBS threshold is near 30 mW of pump power. (b) Stokes amplitude at $z=L$ as a function of time when the input power is near threshold. When the gain is low (29.7 mW), the output is constant in time. As the gain is increased, the output exhibits oscillations with a period equal to the round-trip transit time.

put pump power to decrease correspondingly. The threshold, $G_{th}=6.82$ (30 mW), is consistent with the value expected from the expression, $G_{th}=2|\ln(R)|+2\alpha L$, as given by Gaeta and Boyd [10]. In Fig. 6(b) we show the normalized Stokes amplitude at $z=L$ as a function of time after about 5500 round trips through the fiber. We note that there is barely any noticeable increase in amplitude or gain below the threshold and, more importantly, that the Stokes signal remains continuous (CW). As the pump power or gain increases, the Stokes signal first develops a modulation, the period of which is equal to the round-trip time in the fiber. Eventually, above the threshold, this regular oscillatory behavior gives way to a train of Stokes pulses shown next in Fig. 7.

In Fig. 7 we present the normalized Stokes amplitude at $z=L$, as in Fig. 6(b) but for two different input powers above the threshold. The train of pulses shown is characteristic of a Fabry–Perot cavity. In Fig. 7(a) the pump power is just above the SBS threshold, the pulses are narrow, and their period is still nearly equal to the round-trip transit time in the fiber cavity, $2n_{g0}L/c$. But, as shown in Fig. 7(b), the transmission characteristics change significantly for higher pump powers. As the pump power is increased from 30 to 50 mW, the period between pulses decreases by about 4%, from T_R to 0.96 T_R, and the pulses become broader and asymmetric.

To make more explicit the effect of pump depletion on the shape and period of the Stokes pulses, we present in Fig. 8 the evolution of both the Stokes and pump amplitudes with time at an arbitrary test location ($z=0.8L$, i.e., closer to the input end of the pump). We start with the boundary conditions given in Eq. (18) and after 5500 round trips and investigate the evolution of the CW pump and Stokes pulse amplitudes as they overlap and interact at the test location. Again, we contrast the results for pump powers near and well above the threshold (P_{IN} =30 and 50 mW). At early times, the Stokes pulse having not yet arrived, the pump sweeps past the test location undepleted. At later times, when the pump and Stokes pulse overlap at the test location, the pump undergoes continuous depletion, first to the leading edge of the Stokes pulse and then to its trailing edge at a reduced level. Several features are worth noting in Fig. 8. At low pump powers [Fig. 8(a)], the pump amplitude exhibits a sharp but small drop of about 2% of its initial value, which corresponds to the depletion of the pump by the equally sharp leading edge of the Stokes pulse. It is interesting to note that the inflection point of this sharp drop
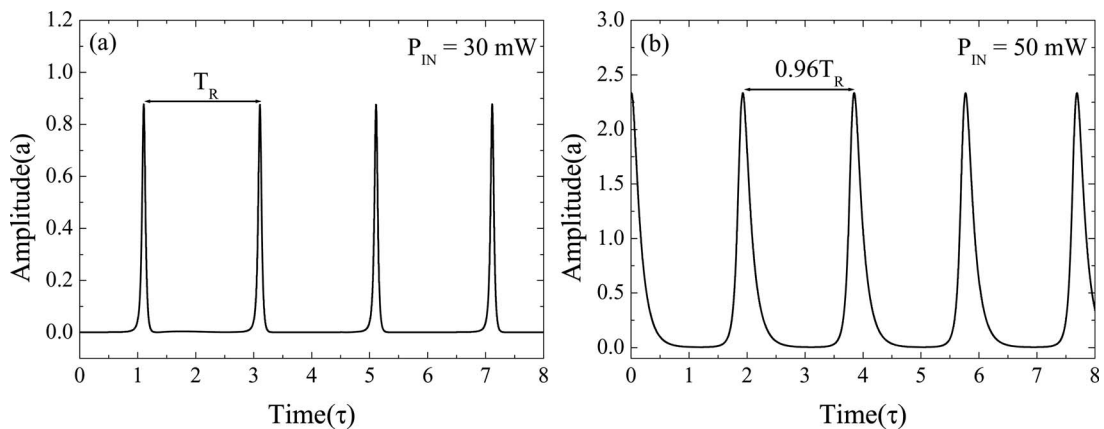

Fig. 7.   Simulation results for the Stokes amplitude at the output end as a function of time. (a) When the pump power is just above the threshold the pulse repetition rate is nearly equal to the round-trip transit time of the passive cavity. (b) At higher pump powers, the transit time decreases suggesting faster light.
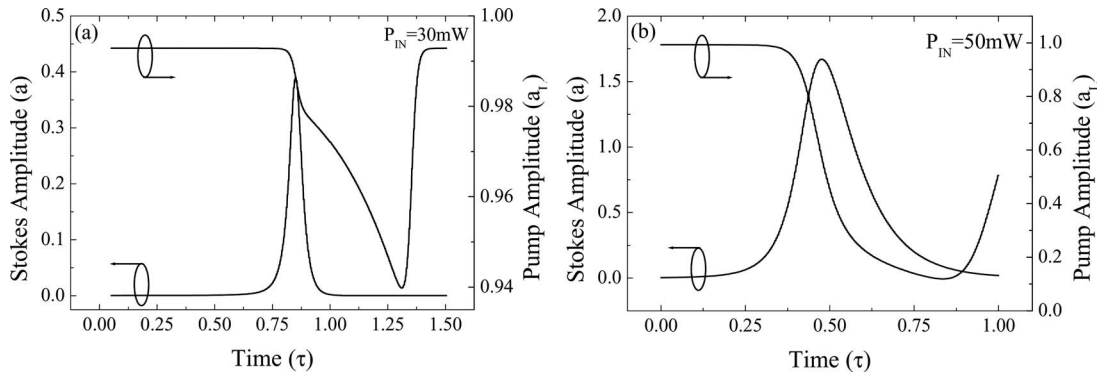
Fig. 8.   Amplitudes of the pump and Stokes light at $z = 0.8L$ as a function of time. (a) Just above the threshold, the pump depletion is a mere 6% of the incident pump power. (b) At higher pump powers the depletion exceeds 80%.

coincides precisely with the maximum of the Stokes pulse (along the time axis). Thereafter, the continued but slower decrease in the amplitude of the pump (as it sweeps past the test location) is the result of the interaction of the pump with the Stokes pulse at points beyond the test location at $z = 0.8L$ as it continues to propagate towards the far end of the fiber at $z = L$. The final rise in the amplitude of the pump reflects the arrival of the single Stokes pulse at the end of the fiber. The final rise time of the pump in fact matches the width of the Stokes pulse. At higher pump powers, as shown in Fig. 8(b), the depletion of the pump becomes significant (about 70%) and both the pump depletion and the Stokes pulse are stretched over a longer time. This stretching is due to the pump being significantly more depleted first by the leading edge and then even further by the trailing edge of the pulse. The leading edge of the pulse sees less depleted pump, and is therefore slowed down as would happen at low-gain, while the trailing edge sees a more depleted pump and is therefore reaccelerated. It is important to note that the trailing edge of the Stokes pulse interact with the counterpropagating pump for longer times than the leading edge, thus receiving additional gain before crossing the test location. For this reason, the trailing edge of the Stokes pulse appears to be stretched. This asymmetry is weak in Fig. 7(a) because of marginal gain at low pump powers. It is important to note that the distortion of the pulse shape is entirely due to the uneven gain across the Stokes pulse.

The essential aspect of the results presented is that the Stokes pulse experiences a continuously changing group

index as it intersects the pump at the test point, because the pump power is being continuously depleted during the crossover. As a consequence, the delay (or change in group index) decreases continuously from the leading edge to the trailing edge of the Stokes pulse.

In Fig. 9 we present the corresponding change in group index, Δn_g, across the Stokes pulse at (a) the same test location as before ($z = 0.8L$) as a function of time and (b) at a given time as a function of axial position along the fiber. In Fig. 9(a), at early times (left side of the figure) when the Stokes pulse has not yet arrived at the test location, the pump is undepleted and Δn_g is at its maximum (about 0.055). As the leading edge of the Stokes pulse (left in the figure) overlaps with the pump at the test location, Δn_g progressively drops from its high value plateau to near zero, when the far end of the trailing edge finally crosses the test location (at later times).

The effect of pump depletion is thus to significantly reduce Δn_g from its undepleted value, thereby reducing the initial slowing down or equivalently reaccelerating the pulse. In Fig. 9(b) we show the change of group index as a function of position along the fiber at a given test time ($\tau = 0.8$) and for the same gain. The curves in this figure are in a sense the mirror image of the curves in Fig. 9(a). The pump is now undepleted at longer distances closer to the end of the fiber, where the group index assumes its maximum value. At intermediate distances, where the Stokes pulse is found interacting with the pump at the test time, the group index first drops due to increasing pump depletion and finally recovers at shorter distances already passed by the Stokes pulse, where the pump re-
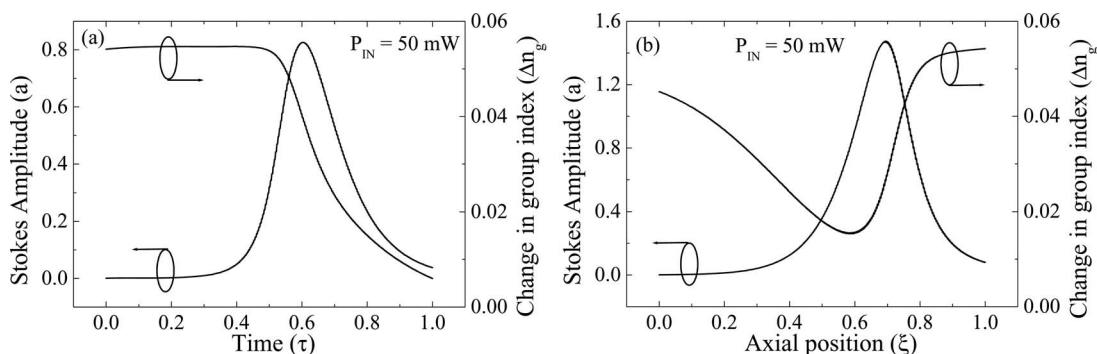

Fig. 9.   Variation of group index across the Stokes pulse. (a) Evolution with time at a fixed $z = 0.8L$, it decreases from 0.05 to 0.02 from the leading edge to the trailing edge. (b) Evolution along the depth of the fiber cavity at a given instant of time, $\tau = 0.8$.
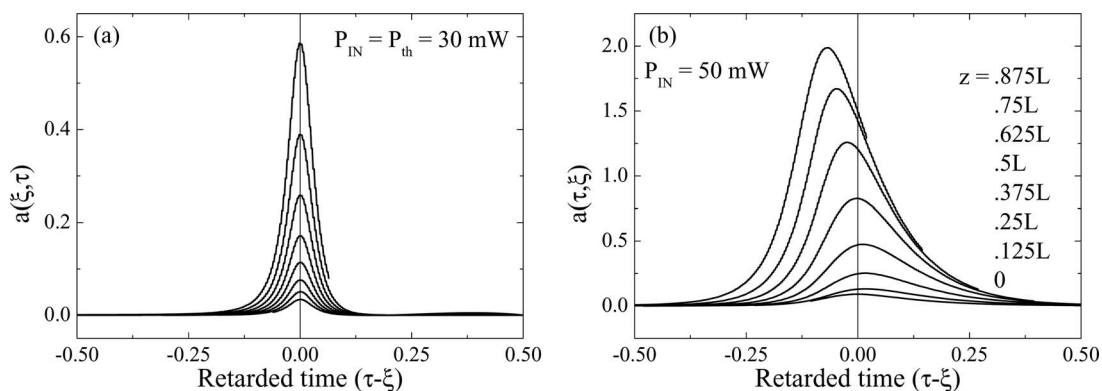
Fig. 10.   Envelope of the Stokes amplitude as a function of the retarded time for various positions along the fiber cavity. (a) Near the threshold, the pulse propagates without any change in group velocity. (b) Above the threshold the pulse propagates with an accelerated group velocity as it approaches the exit or output end.

covers its undepleted value. Thus, the central region of the Stokes pulse experiences a self-induced dip in group index.

The ultimate effect of the nonuniform group velocity across the Stokes pulse uncovered in this study is to re-accelerate the pulse itself. This is more explicitly shown in Fig. 10 where we plot the amplitude of the Stokes pulse as a function of the retarded time $\tau - \xi$ for two different pump powers or equivalently two different gains, one close to the threshold and the other well above it. As the pulse travels its amplitude increases in both cases, although significantly more for the higher gain, as expected. More importantly, for the higher gain the peak of the Stokes pulse, as observed at different points along the fiber cavity, is seen to move to earlier times, indicating that it is being accelerated. This is to be contrasted with what happens in the low-gain regime just above the threshold [see Fig. 10(a)], where the pulse observed at different points along the fiber retains its shape, i.e., all parts of the pulse travel with the same reduced velocity. This is expected because, at low-gain, the pump is being negligibly depleted. For higher gains [Fig. 10(b)], the Stokes pulse experiencing a nonuniform velocity deforms as it propagates and its maximum moves to shorter re-

tarded times. The Stokes pulse is therefore accelerated as it moves towards the end of the fiber cavity.

In view of the results presented in this paper, a final remark may be in order on the use of the term group velocity. As defined in Eq. (1), the group index and therefore the group velocity are well-defined quantities, since the pump intensity I_L is taken to be a constant in the low-gain–undepleted pump regime. As we have shown, in the high-gain–depleted pump regime the pump intensity is no longer a constant across the Stokes pulse but decreases from the leading edge to the trailing edge. The group index and the group velocity consequently also vary across the Stokes pulse, which contributes to its deformation. The Stokes pulse can then be characterized by either an average group velocity or by the velocity of the peak of the Stokes pulse equated to the velocity of its envelope. The latter could also be identified as a signal velocity [33].

The previous figures presented the evolution of the Stokes pulse in the time domain, as it could be observed on an oscilloscope. However, as was mentioned at the beginning of the paper, the initial observation of these effects came from noticing an increase in the cavity mode frequency separation on a spectrum analyzer, and therefore in the frequency domain. To make the final connection between this initial experimental observation and simulation results reported here, we have taken the Fourier transform of the simulated time domain traces of Fig. 7 and the results are shown in Fig. 11. As the pump power is increased, the frequency interval between cavity modes, or equivalently the FSR, is indeed seen to increase. In addition, the frequency separation is no longer constant but it increases with the order of the modes, which, as we have shown, explains the asymmetric distortion of the Stokes pulse as it propagates.
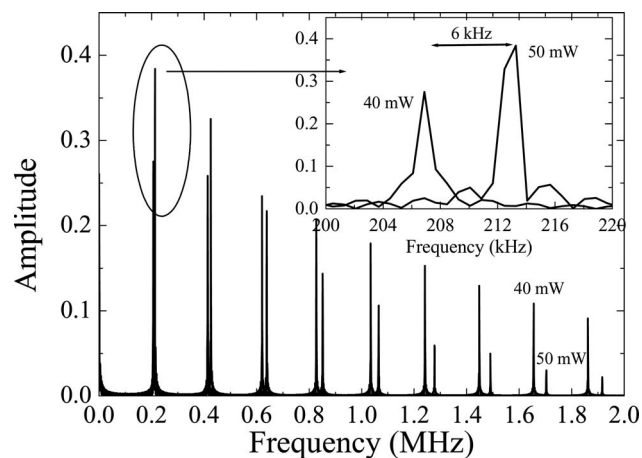

Fig. 11.   Numerically computed frequency spectrum of the Stokes signal. Note that, for 50 mW of input power, the modes appear at higher frequencies than for 40 mW. The inset shows that the first mode shifts by about 6 kHz.

6. CONCLUSION

We have investigated, both numerically and experimentally, the evolution of a Stokes wave as it experiences increasing gain. Earlier studies have reported the use of SBS to slow down the light and have mentioned a saturation effect as the gain increases. In the present paper, we have extended these studies to the high-gain regime of a Brillouin laser and have identified and characterized the

consequences of pump depletion on the shape and propagation of the Stokes signal. We have shown that the transit time of the Stokes pulse through the fiber laser cavity decreases as the pump power is increased, an effect that is also seen as a shift of the resonant cavity modes to higher frequencies. This upward shift of the resonant modes reflects an increase in the group velocity of the Stokes pulse. Numerical simulations reveal that, due to the effect of pump depletion, the Stokes pulse propagates with a nonuniform delay or group index. The group index progressively decreases from the leading edge to the trailing edge of the Stokes pulse as it counterpropagates to the pump, leading to its asymmetric deformation and acceleration. Otherwise stated, the Stokes pulse interacting with the pump through SBS experiences an asymmetric dip in the group index.

ACKNOWLEDGMENTS

REFERENCES

1. N. M. Kroll, "Excitation of hypersonic vibrations by means of photoelastic coupling of high-intensity light waves to elastic waves," J. Appl. Phys. **36**, 34–43 (1965).
2. C. L. Tang, "Saturation and spectral characteristics of the Stokes emission in the stimulated Brillouin process," J. Appl. Phys. **37**, 2945–2955 (1966).
3. V. S. Starunov and I. L. Fabelinskiĭ, "Stimulated Mandel'shtam-Brillouin scattering and stimulated entropy (temperature) scattering of light," Sov. Phys. Usp. **12**, 463–488 (1970).
4. R. W. Boyd, *Nonlinear Optics* (Academic, 1992).
5. E. Picholle, in *Guided Wave Nonlinear Optics*, D. B. Ostrowsky and R. Reinisch, eds. (Kluwer, 1992), pp. 627–647.
6. G. P. Agrawal, *Nonlinear Fiber Optics*, 2nd. ed. (Academic, 1995).
7. D. Cotter, "Observation of stimulated Brillouin scattering in low-loss silica fiber at 1.3 μm," Electron. Lett. **18**, 495–496 (1982).
8. N. Shibata, K. Okamoto, and Y. Azuma, "Longitudinal acoustic modes and Brillouin-gain spectra for GeO2-doped-core single-mode fibers," J. Opt. Soc. Am. B **6**, 1167–1174 (1989).
9. A. Yeniay, J.-M. Delavaux, and J. Toulouse, "Spontaneous and stimulated Brillouin scattering gain spectra in optical fibers," J. Lightwave Technol. **20**, 1425–1432 (2002).
10. A. I. Gaeta and R. W. Boyd, "Stimulated Brillouin scattering in the presence of feedback," Int. J. Nonlinear Opt. Phys. **1**, 581–594 (1992).
11. C. Montes, D. Bahloul, I. Bongrand, J. Botineau, G. Cheval, A. Mamhound, E. Picholle, and A. Picozzi, "Self-pulsing and dynamic bistability in cw-pumped Brillouin fiber ring lasers," J. Opt. Soc. Am. B **16**, 932–951 (1999).
12. Y. Okawachi, M. S. Bigelow, J. E. Sharping, Z. Zhu, A. Schweinsberg, D. J. Gauthier, R. W. Boyd, and A. L. Gaeta, "Tunable all-optical delays via Brillouin slow light in an optical fiber," Phys. Rev. Lett. **94**, 153902–153905 (2005).
13. K. Y. Song, M. González-Herráez, and L. Thévenaz, "Observation of pulse delaying and advancement in optical fibers using stimulated Brillouin scattering," Opt. Express **13**, 82–88 (2005).
14. Z. Zhu, D. J. Gauthier, Y. Okawachi, J. E. Sharping, A. L. Gaeta, R. W. Boyd, and A. E. Willner, "Numerical study of all-optical slow-light delays via stimulated Brillouin scattering in an optical fiber," J. Opt. Soc. Am. B **22**, 2378–2384 (2005).
15. M. González-Herráez, K.-Y. Song, and L. Thévenaz, "Optically controlled slow and fast light in optical fibers using stimulated Brillouin scattering," Appl. Phys. Lett. **87**, 081113 (2005).
16. R. W. Boyd and D. J. Gauthier, "'Slow' and 'fast' light," in *Progress in Optics*, E. Wolf, ed. (Elsevier, 2002), Vol. 43, Chap. 6, pp. 497–530.
17. J. Botineau, C. Leycuras, C. Montes, and E. Picholle, "Stabilization of a stimulated Brillouin fiber ring laser by strong pump modulation," J. Opt. Soc. Am. B **6**, 300–312 (1989).
18. I. Bar-Joseph, A. A. Friesem, E. Lichtman, and R. G. Waarts, "Steady and relaxation oscillations of stimulated Brillouin scattering in single-mode optical fibers," J. Opt. Soc. Am. B **2**, 1606–1611 (1985).
19. A. Yariv, *Optical Electronics* (Holt, Rinehart and Winston, 1976), Chap. 6.
20. M. Dämmig and F. Mitschke, "Velocity of pulse propagation in media with amplitude nonlinearity," Appl. Phys. B, **59**, 345–349 (1994).
21. J. E. McElhenny, R. K. Pattnaik, J. Toulouse, K. Saitoh, and M. Koshiba, "Unique characteristic features of stimulated Brillouin scattering in small-core photonic crystal fibers," J. Opt. Soc. Am. B **25**, 582–593 (2008).
22. M. Dämmig, G. Zinner, F. Mitschke, and H. Welling, "Stimulated Brillouin scattering in fibers with and without external feedback," Phys. Rev. A **48**, 3301–3309 (1993).
23. E. Picholle, C. Montes, C. Leycuras, O. Legrand, and J. Botineau, "Observation of dissipative superluminous solitons in a Brillouin fiber ring laser," Phys. Rev. Lett. **66**, 1454–1457 (1991).
24. D. Yu, W. Lu, and R. G. Harrison, "Physical origin of dynamical stimulated Brillouin scattering in optical fibers with feedback," Phys. Rev. A **51**, 669–674 (1995).
25. V. Lecoeuche, S. Randoux, B. Segard, and J. Zemmouri, "Dynamics of stimulated Brillouin scattering with feedback," Quantum Semiclassic. Opt. **8**, 1109–1145 (1996).
26. C. Montes, A. Mamhmoud, and E. Picholle, "Bifurcation in a cw-pumped Brillouin fiber-ring laser: Coherent soliton morphogenesis," Phys. Rev. A **49**, 1344–1349 (1994).
27. J. Botineau, C. Leycuras, C. Montes, and E. Picholle, "Coherent modal analysis of a Brillouin fiber ring laser," Opt. Commun. **109**, 126–132 (1994).
28. Y. Imai and H. Aso, "Chaos in fiber-optic stimulated Brillouin scattering without external feedback in large nonlinear refractive index regime," Opt. Rev. **4**, 636–638 (1997).
29. Y. Imai and H. Aso, "Chaos in fiber-optic stimulated Brillouin scattering dependent on pump power, nonlinear refractive index, feedback power, and fiber length," Opt. Rev. **4**, 476–480 (1997).
30. C. C. Chow and A. Bers, "Chaotic stimulated Brillouin scattering in a finite-length medium," Phys. Rev. A **47**, 5144–5150 (1993).
31. R. G. Harrison, P. M. Ripley, and W. Lu, "Observation and characterization of deterministic chaos in stimulated Brillouin scattering with weak feedback," Phys. Rev. A **49**, R24–R27 (1994).
32. L. Chen and X. Bao, "Analytical and numerical solutions for steady-state stimulated Brillouin scattering in a single-mode fiber," Opt. Commun. **152**, 65–70 (1998).
33. L. Brillouin, *Wave Propagation and Group Velocity* (Academic, 1960).